IEEE Access
Multidisciplinary ⋮ Rapid Review ⋮ Open Access Journal

Received 30 June 2024, accepted 30 July 2024, date of publication 5 August 2024, date of current version 13 August 2024.

Digital Object Identifier 10.1109/ACCESS.2024.3438121

RESEARCH ARTICLE

Estimation of Carrier Frequency Offset Plagued by IQ Mismatch Using Least-Squares Interpolation of the DFT Coefficients

YIN KUANG[1], SHUXIAO LI[2], XUN HAN[1], WEI WEN[1], YU WANG[1], AND MINGYU LI[3], (Member, IEEE)

[1]Xi'an Branch of China Academy of Space Technology, Xi'an 710000, China
[2]School of National Defence Science and Technology, Southwest University of Science and Technology, Mianyang 621010, China
[3]School of Microelectronics and Communication Engineering, Chongqing University, Chongqing 400044, China

Corresponding author: Mingyu Li (myli@cqu.edu.cn)

This work was supported in part by the Funds in the Field of Technology of the Enhanced Program of National Basic Research under Grant 2022-JCJQ-JJ-0637; in part by the Sustainedly Supported Foundation by the National Key Laboratory of Science and Technology on Space Microwave under Grant HTKJ2022KL504006; in part by the National Natural Science Foundation of China under Grant 62171068, Grant 62371077, and Grant 62171065; and in part by the Science and Technology Research Program of Chongqing Municipal Education Commission, China, under Grant KJQN202304001 and Grant KJQN202201525.

ABSTRACT The rapid development of wireless communication systems demands extremely high reliability in transmission links. However, non-ideal characteristics of RF links, such as carrier frequency offset (CFO) and IQ mismatch (IQM), can lead to RF impairments, severely affecting system performance. Advanced signal processing techniques are indispensable to mitigate the non-ideal characteristics of RF links. Within signal processing, synchronization issues, including CFO estimation schemes for frequency synchronization, should be prioritized. However, the traditional CFO estimation schemes are susceptible to interference from the harmonics caused by IQM, resulting in severe performance degradation. Therefore, based on the least squares (LS) interpolation method, we develop a CFO estimation scheme robust to IQM by using $2l_0+1$ ($l_0 \geqslant 3$) discrete Fourier transform (DFT) coefficients. The proposed estimator combines a coarse estimation and a fine estimation. In the first stage, the peak position of the signal amplitude spectrum is detected to provide a rough frequency estimation. In the second stage (fine estimation), an LS equation relationship between the observation vector and the observation matrix is established with observed DFT samples and DFT rotation factors. The precise frequency is extracted using the LS principle from the equation, utilizing $2l_0+1$ ($l_0 \geqslant 3$) DFT sample points. Because the IQM interference structure is considered in the equation, the proposed method can combat IQI. Test results based on the RF verification platform indicate that the proposed method improves accuracy by at least 20 dB at an input power of -45 dBm. Accuracy improves by at least 9 dB at an input power of -65 dBm. Complexity analysis shows that the proposed method increases by at most 10.74% compared to the traditional LS-based methods.

INDEX TERMS Frequency synchronization, carrier frequency offset, DFT interpolation, IQ mismatch, least squares.

I. INTRODUCTION

With the explosive growth in wireless communication demands, current spectrum resources have become highly congested. One strategy to address this issue is the development of ultra-high-frequency communication, such as the millimeter-wave bands (30 GHz - 300 GHz) used in 5G and the terahertz bands (0.1 THz - 10 THz) considered in 6G [1], [2]. The requirements for achieving ultra-high-frequency communication are that the transmission links possess extremely high performance and reliability. The error requirements for 5G communication systems are as

The associate editor coordinating the review of this manuscript and approving it for publication was Anandakumar Haldorai.

follows: in the Sub-6 GHz bands, the error vector magnitude (EVM) should be less than 0.5%; in the millimeter-wave bands, the EVM should be less than 0.75% [3]. To achieve reliable ultra-high-frequency transmission for current and future communication systems, a significant challenge that must be considered is the non-ideal characteristics of the radio frequency (RF) transmission links, such as carrier frequency offset (CFO) [4], [5], [6], [7], [8], which is caused by the frequency accuracy error of the local oscillator (LO) or Doppler frequency shift [8]. In wireless communication systems, the CFO occupies signal bandwidth, limiting the effective utilization of spectrum resources. Additionally, the frequency offset caused by the CFO mismatches the signal with the receiver's filters, thereby reducing the signal strength and reliability. In orthogonal frequency division multiplexing (OFDM) systems, CFO introduces inter-symbol interference and inter-carrier interference, disrupting the orthogonality between OFDM subcarriers and severely affecting the demodulation performance of OFDM systems [8].

To mitigate the impact of CFO on signal transmission and signal processing, advanced estimation and correction techniques are needed. These estimation schemes can be roughly divided into blind estimation [9], [10], [11] and training sequence estimation [12], [13], [14], [15], [16], [17], [18], [19], [20], [21], [22]. Blind estimation does not require additional training sequences but demands a high signal-to-noise ratio (SNR). Training sequence estimation relies on specific training sequences, offering high estimation accuracy and adaptability to complex transmission environments [10]. In training sequence-based estimation methods, the CFO normalized to subcarrier spacing is typically divided into integer and fractional parts. The former results in periodic signal variations, while the latter causes amplitude and phase distortion. Among these estimation schemes, the maximum likelihood criterion has received particular attention [14], [15]. Typically, two steps are considered to approximate the maximum likelihood (ML) criterion: a coarse search around the normalized CFO integer part and a fine search around the normalized CFO fractional part. However, ML-based CFO estimation involves a complex search process with high computational complexity.

The method proposed in [16] estimates the frequency by searching for the maximum value of the received signal discrete Fourier transform (DFT) magnitude spectrum. However, due to spectral leakage and the picket-fence effect introduced by DFT operations, the performance of this method is suboptimal. Therefore, this method can also be considered as providing only a rough estimate of the normalized CFO integer part.

To provide more accurate frequency estimation with fewer observation sequences, many schemes focus on providing finer estimates of the normalized CFO fractional part through DFT interpolation methods [17], [18], [19], [20], [21], [22]. In [19], a parabolic interpolation method is employed to estimate the residual fractional frequency offset using only three samples near the DFT spectrum peak. The advantage of this method is its simplicity in computation, but its estimation performance is suboptimal. Consequently, many optimized DFT interpolation methods have been proposed. In [20], based on Jacobsen's interpolation scheme, a bias-corrected estimator with superior estimation accuracy is presented. Morelli introduced an estimator based on the weighted least squares (WLS) algorithm, utilizing arbitrary DFT samples [21], which demonstrated higher accuracy than previous techniques when the DFT length was 64. However, the WLS coefficients need to be solved iteratively and the calculation overhead is huge. In [22], an estimator with lower complexity that uses two DFT sample points is proposed. The results demonstrate that the estimator performance will suffer deterioration in the presence of harmonics but did not provide practical solutions.

Nevertheless, the aforementioned techniques ignore RF impairments and only consider thermal noise and channel distortion. In RF broadband transmitters or receivers, quadrature modulation or demodulation structures are widely used benefiting from the improved spectrum utilization at the expense of in-phase and quadrature mismatch (IQM) [23]. Stemming from the imperfections of RF and baseband components in the I and Q branches, IQM causes serious mirror interference. In such systems, IQM is usually entangled with CFO so that the conventional CFO estimation schemes suffer from severe performance degradation [24].

To handle this problem, a great deal of research on CFO estimation with IQM has been conducted. Although the approaches in [25] and [26] are robust to IQM, the lack of a closed-form solution makes them excessively complicated. To this end, the low-complexity methods are presented in [27] and [28]. However, the pilot symbols of these methods are designed according to WLAN standards, limiting their application in synchronization standard-customized systems, such as satellite communications, radar signal processing, pre-distortion systems, and instrumentation testing.

Focusing on the CFO estimation entangled with IQM, this paper presents a fine estimator robust to IQM. Unlike the conventional estimation method, the proposed scheme considers the IQM interference structure in fine estimation. By using the observed DFT samples and the DFT rotation factors, the proposed method establishes an equation for DFT interpolation. The characteristics of the frequency domain impulse response of the single-tone pilot sequence promote the decoupling of the IQM and CFO. Then, the least squares (LS) principle can be employed to solve the coefficients from the equation so that the proposed algorithm provides a closed-form solution. The effectiveness of the proposed algorithm is confirmed through an in-depth analysis of its complexity, extensive simulations, and the validation of experimental outcomes.

The innovations of the proposed method in this paper include: 1) Incorporating the IQM interference structure into the traditional LS interpolation to mitigate the impact of IQM

on CFO estimation. 2) Leveraging the sampling characteristics of single-tone sequences to decouple IQM parameters from CFO parameters in the coefficient equation, thereby simplifying the coefficient-solving process. 3) Utilizing a greater number of DFT sample points to solve the coefficient equation, and resulting in a more accurate CFO estimation value.

The remainder of this paper is organized as follows. The analytical model of IQM with CFO is presented in Section II. The proposed method and the computational complexity are derived in Section III. In Section IV, simulation and experimental results are discussed. Finally, Section V concludes this paper.

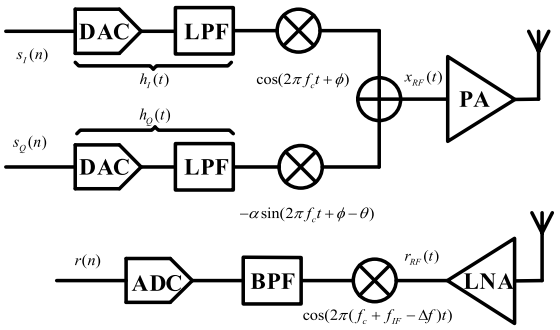

FIGURE 1. The system architecture with IQM and CFO.

II. SYSTEM AND SIGNAL MODEL

An overview of the transceiver architecture with IQM and CFO is shown in Fig. 1, where the IQ transmitter and the following super-heterodyne receiver are considered. In this case, IQM typically occurs in the IQ transmitter with a quadrature up-conversion structure. The CFO is modeled by the difference in carrier frequency between the transmitter and the receiver and denoted by Δf.

Letting $s(n) = s_I(n) + js_Q(n)$ represent the complex, discrete-time, baseband signal, its components $s_I(n)$ and $s_Q(n)$ are fed into the digital-to-analog converters (DACs) and the reconstruction filters with real-valued composite impulse responses $h_I(t)$ and $h_Q(t)$ of the I and Q channels, respectively, whose relative difference results in frequency-dependent IQM. In the quadrature up-converter, the filter output signal is modulated to RF and the RF signal can be expressed as $s_{LO,tx}(t) = \cos(2\pi f_c t) - j\alpha\sin(2\pi f_c t + \phi)$, where f_c represents the carrier frequency. Due to LO's imperfections, the IQ branches usually suffer from an amplitude mismatch and phase errors characterized by α and θ, respectively, giving rise to the frequency-independent imbalance.

Assuming that $x_{RF}(t) = 2\mathrm{Re}\{x(t)s_{LO,tx}(t)\}$ is the RF real-valued bandpass signal, then its corresponding baseband equivalent $x(t) = x_I(t) + jx_Q(t)$ can be modelled as:

$$x(t) = s(t) \otimes g_1(t) + s^*(t) \otimes g_2(t) \tag{1}$$

where $g_1(t)$ and $g_2(t)$ represent the impulse responses associated with the signal and its image, respectively, and expressed as:

$$g_1(t) = [h_I(t) + \alpha e^{-j\theta} h_Q(t)]/2 \tag{2}$$

$$g_2(t) = [h_I(t) - \alpha e^{-j\theta} h_Q(t)]/2 \tag{3}$$

After a succeeding power amplifier common to both I and Q channels and a propagation channel, the received RF waveform $r_{RF}(t)$ is down-converted to baseband in the super-heterodyne receiver with frequency offset Δf. Then the observed baseband complex envelop is expressed as:

$$\begin{aligned} r(t) &= LPF\{r_{RF}(t)e^{-j2\pi(f_c-\Delta f)t}\} \\ &= [x(t) \otimes c(t)]e^{j2\pi\Delta ft} \end{aligned} \tag{4}$$

where $c(t)$ characterize the channel response after up-conversion and before down-conversion. Substituting (1) into (4) yields

$$r(t) = [s(t)e^{j2\pi\Delta ft}] \otimes g_1'(t) + [s^*(t)e^{j2\pi\Delta ft}] \otimes g_2'(t) + q(t) \tag{5}$$

where $g_i'(t) = [g_i(t) \otimes c(t)]e^{j2\pi\Delta ft}$ with $i = 1, 2$, and $q(t)$ represents the overall additive Gaussian white noise.

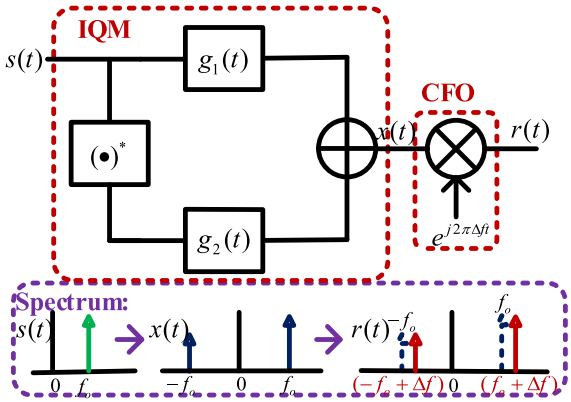

FIGURE 2. The baseband signal model and Spectrum elaboration impacted by IQM and CFO.

In the equation presented above, the first term characterizes the signal component of interest, while the second term accounts for self-interference. Fig. 2 illustrates the analytical model of the IQM system incorporating CFO, accompanied by relevant spectral representations. Assuming the complex baseband signal as a single-tone sequence centered at $(f_c + \Delta f)$, it is important to observe that due to IQM, a spectral component landing at $(-f_c + \Delta f)$ is regenerated within the spectrum of the signal of interest.

III. DFT INTERPOLATION BASED CFO ESTIMATION

A. CONVENTIONAL DFT INTERPOLATION METHOD

The DFT interpolation technique is a commonly employed method in frequency estimation. The conventional frequency estimation methods based on DFT interpolation typically proceed in two steps. In the first stage, the input sequence undergoes an N-point DFT to obtain a rough spectral peak

location. In the second stage, a fine search is conducted around the peak determined in the first stage.

The two-stage estimation is based on the following considerations. First, under a certain signal-to-noise ratio condition, the peak of the discrete-time Fourier transform (DTFT) magnitude spectrum of the observed tone signal corresponds to the true frequency to be estimated. However, due to the high complexity of peak search in the DTFT magnitude spectrum, DFT computations are used in the first stage to obtain a rough peak position. Nonetheless, DFT computations introduce effects such as spectral leakage, resulting in an error between the position of the DTFT magnitude spectrum peak and the DFT magnitude spectrum peak. Therefore, DFT interpolation is required in the second stage to achieve fine-tuning of the search.

A complex exponential observation signal affected by carrier frequency offset in a Gaussian white noise environment is considered and written as:

$$r(n) = Ae^{j(2\pi f_1 nT_s+\varphi)} + q(n), \quad n = 0, 1, \cdots, N-1 \tag{6}$$

where A and φ respectively represent the amplitude and initial phase of the single-tone signal, N is the sample length, $q(n)$ characterizes the noise, and f_1 denotes the initial frequency which can be expressed as:

$$f_1 = f_o + \Delta f \tag{7}$$

where f_o represents the initial frequency CFO.

Notice that f_1 represents the true frequency to be estimated and corresponds to the DTFT magnitude spectrum peak position, which is located between two DFT subcarriers. Due to spectrum leakage and the fence effect, the peak of the DFT magnitude spectrum of $r(n)$ does not align with the true peak position of the DTFT magnitude spectrum. This discrepancy means that f_1 can be expressed as the sum of integer multiples and fractional multiples of the subcarrier spacing, i.e.

$$f_1 = (k_p + \varepsilon)D \tag{8}$$

where $k_p \in [-N/2-1, N/2]$ and $\varepsilon \in [-0.5, 0.5]$ are the integer multiplier and the fractional multiplier respectively. $D = 1/NT_s$ is the subcarrier spacing, and T_s represents the sampling period.

According to (8), the estimation of f_1 can be regarded as the estimation of the integer multiplier k_p and the fractional multiplier ε. The two-stages estimation is performed sequentially.

In the first stage, computing N-point DFT of $r(n)$ yields:

$$R(k) = \sum_{n=0}^{N-1} r(n)W_N^{nk} \tag{9}$$

where $k \in [-N/2-1, N/2]$ represents the subcarrier index of N-point DFT, W_N^k is the rotation factor of DFT which can be expressed as:

$$W_N^k = e^{-j2\pi k/N}. \tag{10}$$

Then the peak position of the DFT magnitude spectrum of $r(n)$ can be obtained by:

$$\hat{k}_p = \arg\max_k(|R(k)|) \tag{11}$$

where $\hat{k}_p$ is the estimation of the integer multiplier k_p.

In the second stage, DFT interpolation method is employed to estimate ε. Applying the following DFT operation on $r(n)$:

$$R_L(k) = \sum_{n=0}^{N-1} r(n)W_N^{n(k+k_p)} \tag{12}$$

then the DFT spectrum peak of $r(n)$ is moved to the position near the subcarrier index $k = 0$. That means that $R_L(0)$ denotes the DFT spectrum peak, $R_L(-1)$ and $R_L(1)$ are the neighbors of $R_L(0)$. Traditional DFT interpolation methods only utilize the three DFT samples near the peak, i.e., $R_L(0)$, $R_L(-1)$, and $R_L(1)$ to estimate the residual frequency offset ε, as referenced in [19], [20], [21], and [22].

B. THE INFLUENCE OF IQM ON DFT INTERPOLATION

The impact of harmonics generated by IQM on the transmitted signal spectrum can be considered from the following two perspectives. On the one hand, due to the need for time-domain truncation of the received signal, the DFT computation at the receiver unavoidably faces the issue of spectral leakage. Additionally, truncating the received signal in the time domain is equivalent to convolving it with a *sinc* function in the frequency domain. Therefore, under the influence of IQM, harmonic interference spills over through convolution with the *sinc* function, disturbing the phase and magnitude of the original received signal DFT samples. On the other hand, in the presence of non-negligible IQI, the energy of the signal leaks to interference harmonics, altering the spectral waveform characteristics of the received signal.

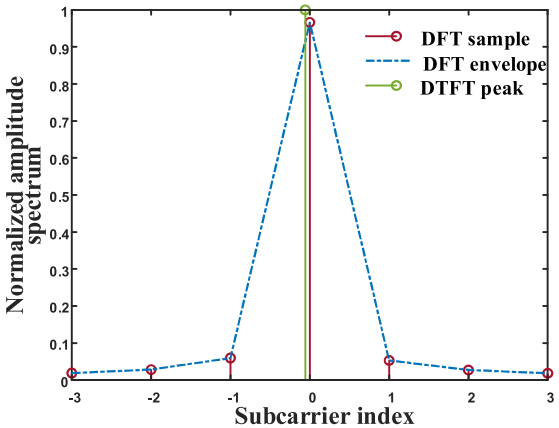

FIGURE 3. The normalized DFT amplitude spectrum (near the peak) of the observed signal without IQM.

Figures 3 and 4 display the signal amplitude spectrum normalized by the maximum of DTFT (DTFT peak) near the peak of the observed tone signal. The frequency spacing between two adjacent DFT samples is $D = 1/NT_s$. A single-path channel model with duplicated impulse responses

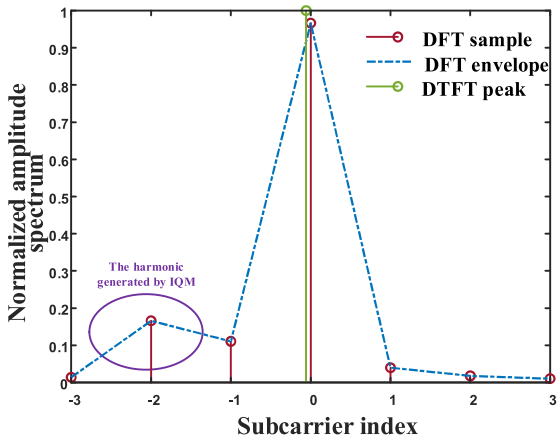

FIGURE 4. The normalized DFT amplitude spectrum (near the peak) of the observed signal with IQM.

between the transmitter and receiver is considered to clarify the effect of IQM on the DFT spectrum. It turns out that in the absence of IQM (when the impulse responses of the I and Q paths are identical), the spectrum of the received signal, as shown in Fig. 3, clearly exhibits only one peak. However, when there is a slight deviation between the impulse responses of the I and Q paths (indicating the presence of IQM), a new frequency component (sub-peak) appears in the received signal spectrum. Furthermore, in the absence of IQM, the energy of the tone signal primarily concentrates on three DFT samples, including the DFT peak and its immediate left and right neighbors. However, as depicted in Fig. 4, in the presence of significant IQM, the signal energy leaks into the harmonics, resulting in the changes of the spectrum waveform. Since the interpolation estimation methods rely on the DFT samples near the spectral peak, any changes in the waveform near the spectral peak will degrade the performance of traditional interpolation methods.

C. PROPOSED ROBUST SCHEME

A single-tone signal with the following discrete-time form is considered as the pilot sequence:

$$s(n) = Ae^{j(2\pi f_o nT_s+\varphi)}, n = 0, 1, \cdots, N-1 \tag{13}$$

Substituting (14) into (5), the observation signal can be written as:

$$r(n) = Ae^{j\varphi}[g_1'(n) \otimes e^{j2\pi f_1 nT_s} + g_2'(n) \otimes e^{j2\pi f_2 nT_s}] + q(n) \tag{14}$$

where $g_1(n)$, $g_2(n)$ and $q(n)$ denote the discrete-time form of $g_1(t)$, $g_2(t)$, and $q(t)$, respectively. f_1 and f_2 respectively represent the center frequencies of the desired signal and the harmonic in the spectrum of the received signal, which can be expressed as:

$$f_1 = f_o + \Delta f, \tag{15}$$
$$f_2 = -f_o + \Delta f. \tag{16}$$

Substituting (15) into (9) yields the N-point DFT of $r(n)$, i.e.

$$\tilde{R}(k) = Ae^{j\varphi}G_1'(k)\frac{1-W_N^{-Nk_1}}{1-W_N^{k-k_1}} + Ae^{j\varphi}G_2'(k)\frac{1-W_N^{-Nk_2}}{1-W_N^{k-k_2}} + Q(k) \tag{17}$$

where $\tilde{R}(k)$ denotes the observed DFT sample on k-th subcarrier which contains the image interference induced by IQM. $k \in \Lambda = [-N/2-1, N/2]$ is the DFT subcarrier index, k_1 and k_2 are the DTFT subcarrier index of f_1 and f_2 respectively, which can be expressed as:

$$k_1 = f_1/D, \tag{18}$$
$$k_2 = f_2/D. \tag{19}$$

$Q(k) = DFT[q(n)]$ is the noise contribution. $G_1'(k)$ and $G_2'(k)$ denote the DFT forms of $g_1'(n)$ and $g_2'(n)$ respectively. Due to the effective bandpass filtering circuitry in signal transmission, DTFT spectrum peak and sidelobe appear respectively at k_1 and k_2.

According to (8), k_1 can be expressed as an integer component k_p, plus a fractional part ε, i.e.

$$k_1 = k_p + \varepsilon \tag{20}$$

where $k_p \in [-N/2-1, N/2]$, $\varepsilon \in [-0.5, 0.5]$.

Since the initial frequency f_o of the single-tone signal is known, the estimation of the carrier frequency offset Δf can be obtained by estimating f_1. Consistent with traditional methods, the estimation of CFO unfolds through two stages of estimation: 1) rough estimation related to the integer multiplier k_p; 2) fine estimation related to the fractional part ε.

Since IQM interference typically does not alter the spectrum peak position of the received sequence, locating peaks on the magnitude spectrum of $r(n)$ can be used to achieve the rough estimation of CFO. Then the estimation of k_p can be obtained by:

$$\hat{k}_p = \arg\max_{k\in\Lambda}(|\tilde{R}(k)|) \tag{21}$$

After obtaining the estimation of integer multiplier k_p, the estimation of fractional multiplier ε is performed by applying the following operation:

$$\tilde{R}_L(l) = \sum_{n=0}^{N-1} r(n)W_N^{n(k_p+l)}, \quad l \in \Gamma \tag{22}$$

where $l \leq N$ denotes the offset of the subcarrier index relative to k_p. By denoting the selected number of DFT sample as l_0 and the center subcarrier index as L_0, then $\Gamma = [-l_0+L_0, l_0+L_0]$ can be viewed as a set of $2l_0+1$ offsets, which specifies that the selected DFT samples utilized for DFT interpolation in the fine estimation stage are $[\tilde{R}_L(L_0-l_0), \cdots, \tilde{R}_L(L_0+l_0)]$.

Submitting (15) into (23), (23) can be reformulated as:

$$\tilde{R}_L(l) = v_1(l)\sum_{n=0}^{N-1} e^{j2\pi f_1 nT_s} W_N^{n(\hat{k}_p+l)} + v_2(l)\sum_{n=0}^{N-1} e^{j2\pi f_2 nT_s} W_N^{n(\hat{k}_p+l)} + Q_L(l) \quad (23)$$

where $v_1(l)$ and $v_2(l)$ represent the filtering parameters of the desired signal and the harmonic respectively, which can be written as:

$$v_i(l) = Ae^{j\varphi}\sum_{n=0}^{N-1} g_i'(n) W_N^{n(k_p+l)}, \quad i = 1, 2. \quad (24)$$

$Q_L(l)$ represents the influence of the noise on DFT interpolation, expressed as:

$$Q_L(l) = \sum_{n=0}^{N-1} q(n) W_N^{n(k_p+l)}. \quad (25)$$

In (24), note that $v_1(l)$ and $v_2(l)$ respectively filter the single-tone signal source and the single-tone interference source. Considering the frequency domain sampling characteristics of the single-tone signal, $v_1(l)$ and $v_2(l)$ can be approximated as constant values υ_1 and υ_2, respectively. After setting $\eta = k_2 - k_p$, (24) can be simplified as:

$$\tilde{R}_L(l) = \upsilon_1 \frac{1 - W_N^{N\varepsilon}}{1 - W_N^{l-\varepsilon}} + \upsilon_2 \frac{1 - W_N^{N\eta}}{1 - W_N^{l-\eta}} + Q_L(l), l \in \Gamma. \quad (26)$$

After performing some standard algebraic operations, the above equation can be transformed into:

$$\begin{aligned}\tilde{R}_L(l) = {} & (W_N^{l-\varepsilon} + W_N^{l-\eta})\tilde{R}_L(l) - W_N^{\varepsilon-\eta}\tilde{R}_L(l)W_N^{2l} \\ & - (\upsilon_1 W_N^{-N\varepsilon} + \upsilon_2 W_N^{-N\eta})W_N^{Nl} \\ & - (\upsilon_1 W_N^{-\eta} + \upsilon_2 W_N^{-\varepsilon})W_N^{l} \\ & + (\upsilon_1 W_N^{-N\varepsilon-\eta} + \upsilon_2 W_N^{-\varepsilon-N\eta})W_N^{Nl+l} \\ & + \upsilon_1 + \upsilon_2 + Q_L'(l) \end{aligned} \quad (27)$$

with $Q_L'(l) = Q_L(l)(1 - W_N^{l-\varepsilon} - W_N^{l-\eta} + W_N^{2l-\varepsilon-\eta})$. Then (27) can be represented in the following matrix form:

$$\tilde{\mathbf{R}}_L = \mathbf{P}\mathbf{c} + \mathbf{Q}_L \quad (28)$$

where $\tilde{\mathbf{R}}_L = [\tilde{R}_L(L_0 - l_0), \tilde{R}_L(L_0 - l_0 + 1), \cdots, \tilde{R}_L(L_0 + l_0)]^T$ is the observation vector of length $2l_0 + 1$. The vector $\mathbf{Q}_L = [Q_L(L_0 - l_0), Q_L(L_0 - l_0 + 1)\cdots, Q_L(L_0 + l_0)]^T$ denotes the noise contribution. $\mathbf{P}$ is a $(2l_0 + 1) \times 6$-dimensional observation matrix. Abbreviating $\tilde{R}_L(l)$ as $\tilde{R}_L^l$, $\mathbf{P}$ can be expressed as:

$$\mathbf{P} = \begin{bmatrix} R_L^{-l_0}W_N^{-l_0} & R_L^{-l_0}W_N^{-2l_0} & W_N^{-Nl_0} & W_N^{-l_0} & W_N^{-Nl_0-l_0} & 1 \\ \vdots & \vdots & \vdots & \vdots & \vdots & 1 \\ R_L^{l}W_N^{l} & R_L^{l}W_N^{2l} & W_N^{Nl} & W_N^{l} & W_N^{Nl+l} & 1 \\ \vdots & \vdots & \vdots & \vdots & \vdots & 1 \\ R_L^{l_0}W_N^{l_0} & R_L^{l_0}W_N^{2l_0} & W_N^{Nl_0} & W_N^{l_0} & W_N^{Nl_0+l_0} & 1 \end{bmatrix}. \quad (29)$$

TABLE 1. Complexity of different estimators with $N = 1024$, $\rho_1 = 7$, $\rho_2 = 3$, $R = 20$, $K = 16$.

Estimator	Amount of real multiplications	Numerical example
PE	$2N\log_2 N + 37$	20517
CLSE	$2N\log_2 N + 56\rho_2 + 144$	20780
ZPE	$2NR\log_2 NR$	586626
POIE	$(8N_s + 2)O$	1300
NLSE	$4K[(N_s + 2)O + 8O + 8]$	120832
proposed	$2N\log_2 N + 176\rho_1 + 1008$	22720

$\mathbf{c} = [c_1, c_2, c_3, c_4, c_5, c_6]^T$ is a vector with $c_1 - c_6$ denoted as:

$$\begin{cases} c_1 = W_N^{-\varepsilon} + W_N^{-\eta} \\ c_2 = -W_N^{-\varepsilon-\eta} \\ c_3 = -\upsilon_1 W_N^{-N\varepsilon} - \upsilon_2 W_N^{-N\eta} \\ c_4 = -\upsilon_1 W_N^{-\eta} - \upsilon_2 W_N^{-\varepsilon} \\ c_5 = \upsilon_1 W_N^{-N\varepsilon-\eta} + \upsilon_2 W_N^{-\varepsilon-N\eta} \\ c_6 = \upsilon_1 + \upsilon_2. \end{cases} \quad (30)$$

Note that when $l_0 \geq 3$, $\mathbf{P}$ is a column full rank matrix. According to (28), the LS solution of $\mathbf{c}$ is:

$$\mathbf{c} = (\mathbf{P}^H\mathbf{P})^{-1}\mathbf{P}^H\tilde{\mathbf{R}}_L \quad (31)$$

Due to the fact that $\varepsilon > \eta$ when $f_o > 0$. Then the estimation of ε can be obtained by:

$$\hat{\varepsilon} = \frac{N}{4\pi}\mathrm{Im}(\ln(c_1 + \sqrt{c_1^2 - 4c_2})). \quad (32)$$

Since the DFT samples closer to the spectral peak suffer the least interference from spectrum leakage, in order to provide a better CFO estimate, $2l_0 + 1$ DFT samples that are symmetrical about the spectral peak are given priority, that is $L_0 = 0$, the corresponding DFT sample set is $[\tilde{R}_L(-l_0), \tilde{R}_L(-l_0 + 1), \cdots, \tilde{R}_L(l_0)]$.

D. COMPLEXITY ANALYSIS

The complexity analysis is carried out based on the real multiplications in the process of frequency estimate. For the proposed estimator, a coarse estimation requires N-point DFT, which generates $(N/2)\log_2 N$ complex product and thus consumes $2N\log_2 N$ real multiplication resources. Then, the calculation amount of fine estimation is reflected in solving (28), including the construction of matrix $\mathbf{P}$ from (29) and LS solution from (31). Considering that the calculation of trigonometric functions can be implemented through lookup tables, the complexity of calculating the exponential factor W_N^k and extracting Δf from $\hat{\varepsilon}$ can be ignored. Then the complexity of (29) is $8\rho_1$, where $\rho_1 = 2l_0 + 1$ represents the number of observed continuous DFT samples. Solving the LS problem of (31) using the Cholesky decomposition requires about $4[\sigma_1^2(\sigma_1 + \rho_1 + 1) + \sigma_1\rho_1]$ real multiplications, in which σ_1 is the number of coefficients of $\mathbf{c}$.

For comparison, the overall complexity of a couple of CFO estimators is summarized in Table 1. These include:

1) the proposed method, 2) the conventional least squares estimator (CLSE) [21], 3) the R-times zero padding based fast Fourier transform (FFT) estimator (ZPE) [16], 4) the parabolic interpolation-based estimator (PE) [19], 5) the nonlinear LS estimator (NLSE) [25], 6) the pseudo-offset injection-based estimator (POIE) [27].

Note that the cost of fine estimation is negligible relative to the FFT operation in coarse estimation for first four single-tone-based estimators. Meanwhile, the proposed method incorporating IQM introduces a slight complexity increase of 10.74% in fine search compared to PE, which is an inevitable result of enhancing the robustness of IQM. The last two lines report two CFO estimators with IQM based on the OFDM pilot sequence adopting the WLAN standard of $O = 16$ pilot symbols and $N_S = 16$ subcarriers for each symbol. NLSE uses iterative interval search, whose complexity is determined by the number of search intervals K. In any case, it is much more demanding than the single-tone-based estimators (the first four estimators in Table 1). POIE uses an approximate sequence correlation algorithm, reducing complexity but presents limiting performance [28]. In the next section, the effective of the proposed estimator is demonstrated by extensive numerical simulations and experiments. Together with the complexity analysis, it will be shown that the proposed algorithm has a good trade-off between complexity and performance.

IV. NUMERICAL RESULTS AND DISCUSSION

A. SIMULATION RESULTS

Comprehensive simulation tests based on MATLAB were carried out to confirm the estimation performance of the suggested algorithm. The statistical performance of the estimator is assessed using the mean square error (MSE) of the CFO estimation normalized by subcarrier spacing and the subcarrier spacing is denoted as $D = 1/NT_s$. In simulation, the sampling period T_s is set to 50 ns. A frequency selective fading channel is employed, in which the impulse response is denoted by $c(n) = [e^{j1.38}, 0.5e^{j0.30}, 0.3e^{-j2.02}]^T$. To examine the impact of IQM on algorithm performance, two IQM scenarios are considered [26]:

Case A): relatively small IQM condition, in which impulse responses of analog IQ filters is $h_I(n) = h_Q(n) = 1$ and LO-induced imbalance is characterized by $\alpha = 0.2dB, \theta = 1°$.

Case B): severe IQM condition with $h_I(n) = [0, 1]^T$, and $\alpha = 1dB, \theta = 5°$.

In addition, each scenario considers SNR traversal and frequency offset traversal at the carrier frequency of $f_c = 2.4$ GHz. When exploring the impact of SNR, values from 10 to 40 dB will be considered. When traversing frequency offset, a typical low-cost oscillator instability of 50 parts-per-million (ppm) is set to the maximum frequency offset. To further validate the sensitivity of the estimator to IQ mismatch parameters, the MSE of different estimators are also measured under varying conditions of gain error and phase error. The gain error factor α changes from -2 to 2 dB, and the phase error varies from $-20°$ to $20°$.

Moreover, the proposed estimator, CLSE, PE, ZPE, NLSE, and POIE are used as simulation objects. For the first four single-tone-based estimators (the proposed, PE, CLSE, and ZPE), set the initial frequency $f_o = 17.5$ kHz and the data sample length $N = 1024$. In the proposed method, the FFT size N during the coarse search stage is set to 1024, and the observation length l_0 during the fine search stage is fixed at 3, consistent with CLSE and PE. Meanwhile, the FFT size for ZPE is set to 20480. The OFDM-based estimators (POIE and NLSE) adhere to the WLAN standard format, with their parameter settings referenced in [28].

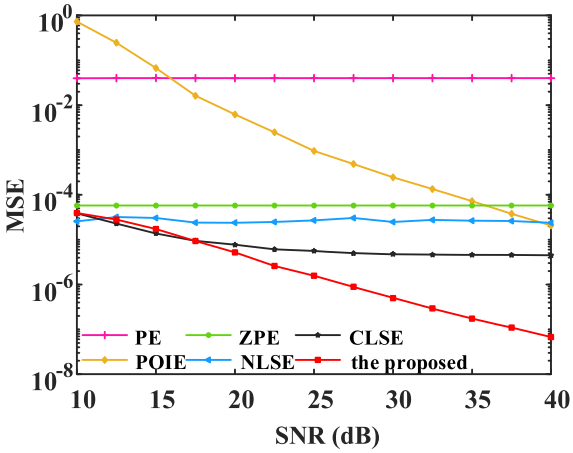

FIGURE 5. MSE of CFO estimation algorithms with different SNR values under case A.

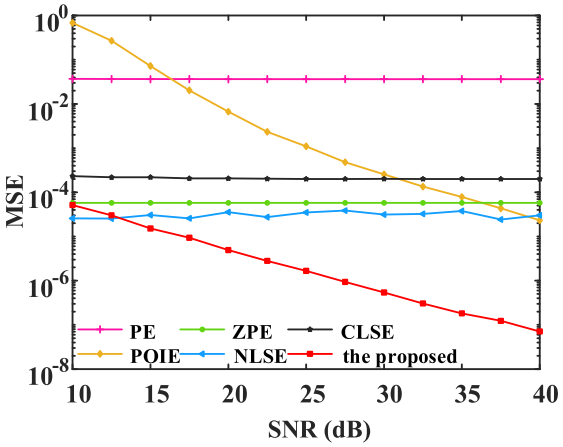

FIGURE 6. MSE of CFO estimation algorithms with different SNR values under case B.

Fig. 5 and Fig. 6 plot the MSE of CFO estimators as a function of different input SNR values under cases A and B, respectively. As is shown, the proposed method exhibits monotonic decline and optimal performance in any scenario. Although the curve of POIE has the same trend as the proposed method, its accuracy is unreliable. The curves of ZPE and NLSE show a relatively stable trend but maintain a poor error level.

The reasons can be explained in sequence. For ZPE, the FFT method based on zero padding can only increase the number of frequency domain sampling points rather than the effective signal length and, therefore, cannot improve physical resolution. For NLSE, although the complex search process related to IQM is considered, the range of search intervals limits estimation accuracy. In addition, it also turns out that the performance of CLSE deteriorates severely in Case B while the proposed method works well under not only slight but also severe IQM conditions. This is thanks to the IQ interference structure considered in the fine search stage. It is worth observing that, under mild IQM scenarios (Case A), the proposed method exhibits performance close to CLSE at low SNR values. The reason is that higher noise power masks lower interference components induced by IQM.

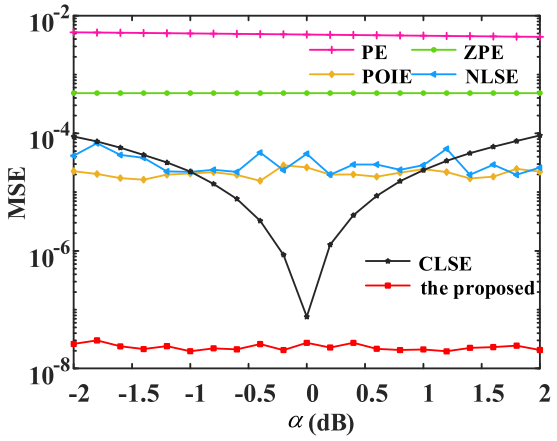

FIGURE 7. MSE of estimation algorithms under different gain errors α.

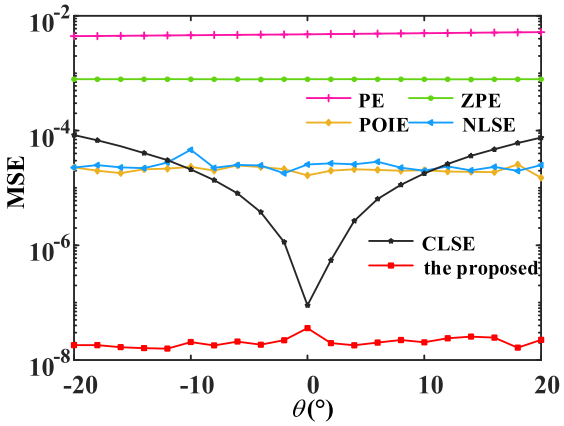

FIGURE 8. MSE of estimators under different phase errors θ.

The accuracy of estimators versus CFO (ppm) is illustrated in Fig. 7 and Fig. 8. As shown, the proposed method outperforms the others across the frequency range considered. Furthermore, the fluctuation observed in the curve of ZPE with the initial CFO depends on the proximity of the estimated value of k_1 to the integer multiples of subcarrier spacing. In comparison, CLSE performs better with smaller fluctuation amplitudes, which implies that the estimation algorithm with DFT interpolation is less dependent on the specific value of CFO than the zero-padding-based approach. This advantage is also evident in the performance of the proposed technique, which incorporates DFT interpolation. Furthermore, the significant enhancement in accuracy achieved by the proposed method is attributed to its ability to mitigate the influence of the regenerated spectral component.

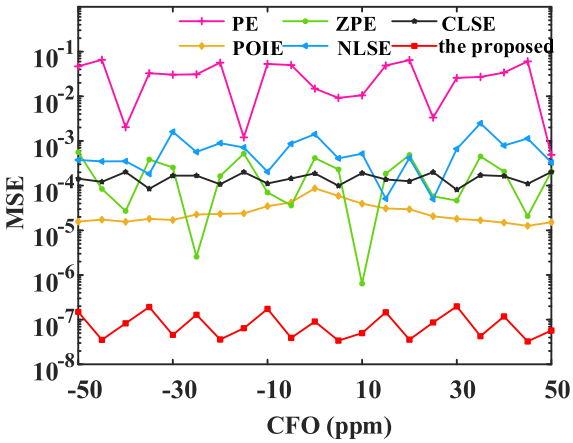

FIGURE 9. MSE of CFO estimators with different CFO under case B.

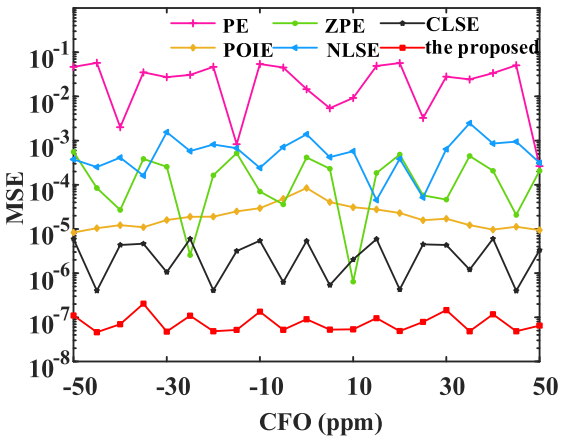

FIGURE 10. MSE of CFO estimators with different CFO under case A.

Fig. 9 illustrates the variation of MSE with the gain imbalance factor α. Set the CFO to 25 ppm, SNR to 40 dB, and θ to 0.2°. Fig 10 depicts the variation of MSE with the phase error factor θ, with α fixed at a very small value of 0.02 dB. As shown in Fig. 9, the estimation errors of both POIE and NLSE are close, with POIE slightly outperforming NLSE. The MSE curve of CLSE exhibits a significant change with α, where the estimation error decreases as α approaches 0, but sharply deteriorates as α increases to ± 2 dB. The suggested method maintains stable estimation accuracy even as α varies, consistently achieving minimal error levels.

It also turns out that CLSE and the proposed method exhibit similar trends in Fig. 10. This indicates that CLSE is effective only when the IQ mismatch is very low or absent, while the

TABLE 2. Performance of different estimators.

Estimator	Interference Structure	Estimated accuracy	Sensitivity to CFO	Robustness to IQM
PE	No	Worst	Highest	Poorest
CLSE	No	Good	High	Good
ZPE	No	Poor	High	Poor
POIE	Yes	Poor	Low	Poor
NLSE	No	Poor	High	Poor
proposed	Yes	Best	Lowest	Best

proposed estimator provides optimal estimation under any IQ mismatch condition. The reason behind this phenomenon is that CLSE does not consider the interference structure of IQM in DFT interpolation. Due to its DFT observation samples are distorted by harmonic interference, the accuracy of DFT interpolation for CLSE depends on the harmonic influence. In contrast, the proposed estimator considers the interference structure of IQM in DFT interpolation, thereby mitigating the impact of IQM on estimation performance even with distorted DFT observation samples.

The performance of the estimator is summarized in Table 2. The estimation accuracy is reflected by the MSE value. Figures 5 to 10 show that the MSE value of PE exceeds 10^{-2}, indicating the worst accuracy. The MSE curves of ZPE, NLSE, and POIE fluctuate above 10^{-5} demonstrating the poor performance. The CLSE method performs slightly better than ZPE, NLSE, and POIE. Overall, the proposed method exhibits the best estimation accuracy.

Figures 7 to 8 reveal that the proposed method has the lowest sensitivity to CFO among these methods,. Although the MSE curve of POIE is the flattest, its estimation accuracy is lower than that of the proposed method. Figures 9 to 10 show that the proposed method demonstrates the best robustness to IQM. The MSE curve of CLSE varies significantly with IQ mismatch conditions, but within a large IQM variation range, its estimation error is lower than that of POIE and NLSE, indicating better performance.

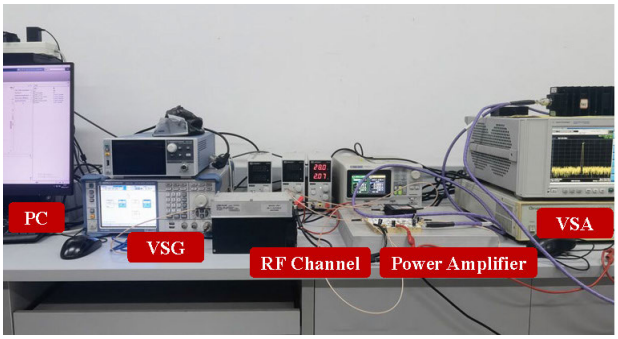

FIGURE 11. Verification platform.

B. MESUREMENT RESULTS

Measurements are also carried out to prove the effectiveness of the investigated scheme in RF applications. A verification platform with RF signals and components is shown in Fig. 11. The baseband pilot signal is generated by a PC and downloaded to the SMB100A vector signal generator (VSG), where the IQ modulation mode is configured, and the IQ imbalance parameters $\alpha = 1$dB and $\theta = 5°$ are applied. The VSG modulates the baseband pilot signal to RF frequency $f_c = 2.4$ GHz, which is then repeatedly played with tunable output power levels.

A vector signal analyzer (VSA) of type Agilent N9000A CXA centered at $f_c - \Delta f$ collects the RF output for down-converting to baseband and digital sampling. The resulting discrete-time digital signal is finally fed into the PC, where the estimator is run after removing the time delay. The estimator parameters similar to those in simulation.

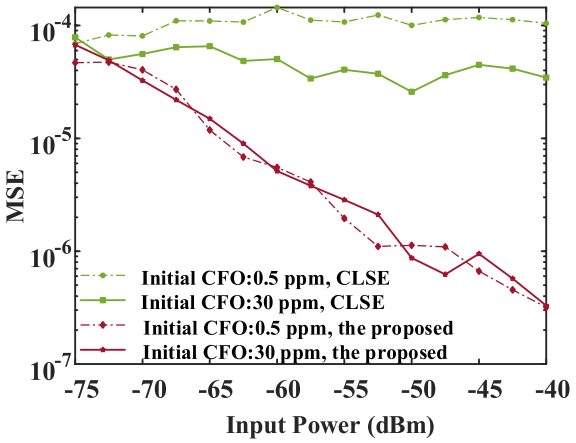

FIGURE 12. Measured MSE versus input Power.

Fig. 12 illustrates the MSE of PLSE and CLSE as a function of the signal input power. As expected, the error curve of the proposed method significantly decreases with the input power increase, while CLSE is plagued by an error floor, maintaining a poor level. Such a discrepancy can be explained by considering the main causes of the estimation error, i.e., the noise and the IQM. Under low input power, the estimation error is dominated by noise disturbances, so the performance of the proposed method is poor and close to CLSE. However, as the input power increases, the interference of IQM leads to errors, and the fine estimation model considering IQM in the proposed method becomes effective.

Fig. 13 depicts the accuracy of the two estimators for different initial CFO. Each estimator is evaluated with an input power of −65 dBm and −45 dBm. The results show that the proposed approach outperforms CLSE in all considered CFO values, with a gain of approximately 9 dB at an input power −65 dBm and 20 dB at an input power −45 dBm.

To further evaluate the impact of estimators on demodulation performance, an OFDM signal (512 subcarriers) is tested on the platform. An efficient IQ imbalance compensation algorithm presented in [23] is considered. Fig. 14 and Fig. 15 plot the constellation of demodulated signals at the input power level of −45 dBm with frequency correction

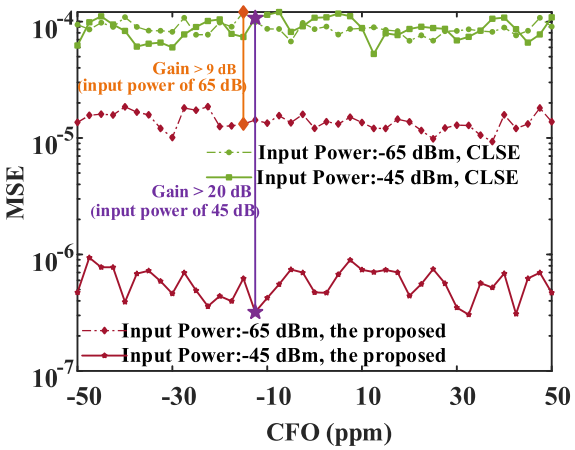

FIGURE 13. Measured MSE versus CFO.

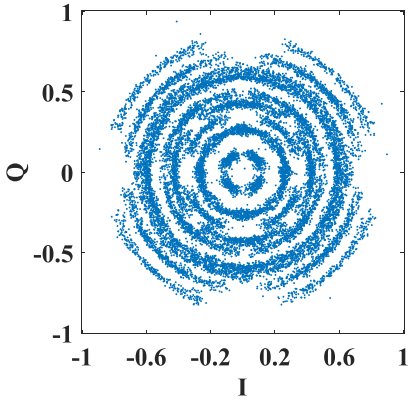

FIGURE 14. Constellation of demodulated signals with CFO corrected by CLSE.

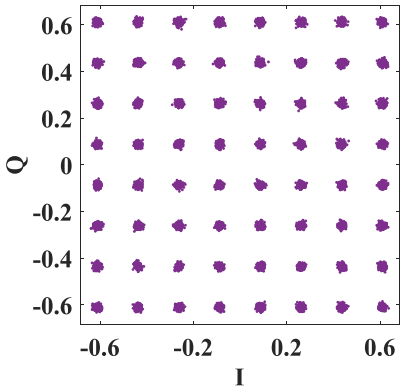

FIGURE 15. Constellation of demodulated signals with CFO corrected by the proposed method.

of the proposed algorithm and CLSE, respectively. It is clearly seen that the symbol points in Fig. 14 are displaced at different times and connected into arcs caused by the residual frequency offset estimated by CLSE, while Fig. 15 provides a more easily distinguishable constellation. This is because the estimation accuracy of CLSE is affected by IQM, resulting in residual frequency offset in the demodulated signal after CLSE correction, leading to constellation rotation in Fig. 14. However, for PLSE, due to its interference-resistant structure, the impact of IQM is alleviated, providing more accurate frequency offset estimation. As a result, the residual frequency offset in the demodulated signal is small after frequency offset correction using PLSE, thus a clearer constellation is presented in Fig. 15.

V. CONCLUSION

In this paper, the interference of IQM on the CFO estimation is investigated in detail. A fine search scheme based on DFT interpolation is proposed to extract the CFO estimate after roughly locating the position of the maximum spectral peak of the single-tone signal. Considering the IQ interference structure in DFT interpolation, the proposed method is robust to IQM. Then, the DFT interpolation coefficients are solved through the LS rule. Complexity analysis and numerical results demonstrate that the proposed algorithm exhibits a good compromise between accuracy and complexity.

REFERENCES

[1] T. M. Getu, G. Kaddoum, and M. Bennis, "A survey on goal-oriented semantic communication: Techniques, challenges, and future directions," *IEEE Access*, vol. 12, pp. 51223–51274, 2024.

[2] M. Jokinen, O. Kursu, N. Tervo, A. Pärssinen, and M. E. Leinonen, "Over-the-air phase calibration methods for 5G mmW antenna array transceivers," *IEEE Access*, vol. 12, pp. 28057–28070, 2024.

[3] E. I. Adegoke, E. Kampert, and M. D. Higgins, "Channel modeling and over-the-air signal quality at 3.5 GHz for 5G new radio," *IEEE Access*, vol. 9, pp. 11183–11193, 2021.

[4] C. P. Davey, I. Shakeel, R. C. Deo, S. Salcedo-Sanz, and J. Soar, "Using sequence-to-sequence models for carrier frequency offset estimation of short messages and chaotic maps," *IEEE Access*, vol. 10, pp. 119814–119825, 2022.

[5] M. Hussien, A. Abdelmoaty, M. Elsaadany, M. F. A. Ahmed, G. Gagnon, K. K. Nguyen, and M. Cheriet, "Carrier frequency offset estimation in 5G NR: Introducing gradient boosting machines," *IEEE Access*, vol. 11, pp. 34128–34137, 2023.

[6] F. Steinmetz and B.-C. Renner, "Doppler shift and SFO robust synchronization for LoRa-like acoustic underwater communication," *IEEE Access*, vol. 11, pp. 130527–130547, 2023.

[7] C. Yang, L. Wang, C. Peng, S. Zhang, Y. Cui, and C. Ma, "A robust time-frequency synchronization method for underwater acoustic OFDM communication systems," *IEEE Access*, vol. 12, pp. 21908–21920, 2024.

[8] A. Mohammadian and C. Tellambura, "RF impairments in wireless transceivers: Phase noise, CFO, and IQ imbalance—A survey," *IEEE Access*, vol. 9, pp. 111718–111791, 2021.

[9] L. Yang, H. Zhang, Y. Cai, and H. Yang, "Blind carrier frequency offset estimation for MIMO-OFDM systems based on the banded structure of covariance matrices for constant modulus signals," *IEEE Access*, vol. 6, pp. 51804–51813, 2018.

[10] A. Rotem and R. Dabora, "A novel low-complexity estimation of sampling and carrier frequency offsets in OFDM communications," *IEEE Access*, vol. 8, pp. 194978–194991, 2020.

[11] W. Chen, A. Liu, X. Liang, T. Yue, and H. Liang, "Blind CFO estimator for OTFS systems in vehicle-to-infrastructure communications," *IEEE Wireless Commun. Lett.*, vol. 12, no. 12, pp. 2048–2052, Dec. 2023.

[12] A. A. D'Amico, M. Morelli, and M. Moretti, "Periodic preamble-based frequency recovery in OFDM receivers plagued by I/Q imbalance," *IEEE Trans. Wireless Commun.*, vol. 16, no. 12, pp. 8305–8315, Dec. 2017.

[13] J. Li, G. Liu, and G. B. Giannakis, "Carrier frequency offset estimation for OFDM-based WLANs," *IEEE Signal Process. Lett.*, vol. 8, no. 3, pp. 80–82, Mar. 2001.

[14] M. D. Macleod, "Fast nearly ML estimation of the parameters of real or complex single tones or resolved multiple tones," *IEEE Trans. Signal Process.*, vol. 46, no. 1, pp. 141–148, Jan. 1998.

[15] F. Horlin, A. Bourdoux, and L. Van Der Perre, "Low-complexity EM-based joint acquisition of the carrier frequency offset and IQ imbalance," *IEEE Trans. Wireless Commun.*, vol. 7, no. 6, pp. 2212–2220, Jun. 2008.
[16] B. F. Beidas, "Radio-frequency impairments compensation in ultra high-throughput satellite systems," *IEEE Trans. Commun.*, vol. 67, no. 9, pp. 6025–6038, Sep. 2019.
[17] Y. Xia, Y. He, K. Wang, W. Pei, Z. Blazic, and D. P. Mandic, "A complex least squares enhanced smart DFT technique for power system frequency estimation," *IEEE Trans. Power Del.*, vol. 32, no. 3, pp. 1270–1278, Jun. 2017.
[18] K. Wang, L. Wang, B. Yan, and H. Wen, "Efficient frequency estimation algorithm based on chirp-Z transform," *IEEE Trans. Signal Process.*, vol. 70, pp. 5724–5737, 2022.
[19] P. Voglewede, "Parabola approximation for peak determination," *Global DSP Mag.*, vol. 3, no. 5, pp. 13–17, 2004.
[20] Ç. Candan, "A method for fine resolution frequency estimation from three DFT samples," *IEEE Signal Process. Lett.*, vol. 18, no. 6, pp. 351–354, Jun. 2011.
[21] M. Morelli, M. Moretti, and A. A. D'Amico, "Single-tone frequency estimation by weighted least-squares interpolation of Fourier coefficients," *IEEE Trans. Commun.*, vol. 70, no. 1, pp. 526–537, Jan. 2022.
[22] K. Wang, H. Wen, and G. Li, "Accurate frequency estimation by using three-point interpolated discrete Fourier transform based on rectangular window," *IEEE Trans. Ind. Informat.*, vol. 17, no. 1, pp. 73–81, Jan. 2021.
[23] H. Yang, W.-J. Shin, S. Lee, and Y.-H. You, "A robust estimation of residual carrier frequency offset with I/Q imbalance in OFDM systems," *IEEE Trans. Veh. Technol.*, vol. 64, no. 3, pp. 1254–1259, Mar. 2015.
[24] A. A. D'Amico, L. Marchetti, M. Morelli, and M. Moretti, "Frequency estimation in OFDM direct-conversion receivers using a repeated preamble," *IEEE Trans. Commun.*, vol. 64, no. 3, pp. 1246–1258, Mar. 2016.
[25] G. Xing, M. Shen, and H. Liu, "Frequency offset and I/Q imbalance compensation for direct-conversion receivers," *IEEE Trans. Wireless Commun.*, vol. 4, no. 2, pp. 673–680, Mar. 2005.
[26] M.-F. Sun, J.-Y. Yu, and T.-Y. Hsu, "Estimation of carrier frequency offset with I/Q mismatch using pseudo-offset injection in OFDM systems," *IEEE Trans. Circuits Syst. I, Reg. Papers*, vol. 55, no. 3, pp. 943–952, Apr. 2008.
[27] X. Wang, F. Ye, and J. Ren, "Comments on 'estimation of carrier frequency offset with I/Q mismatch using pseudo-offset injection in OFDM systems,'" *IEEE Trans. Circuits Syst. I, Reg. Papers*, vol. 59, no. 11, pp. 2795–2798, Nov. 2012.
[28] H. Lin, X. Zhu, and K. Yamashita, "Low-complexity pilot-aided compensation for carrier frequency offset and I/Q imbalance," *IEEE Trans. Commun.*, vol. 58, no. 2, pp. 448–452, Feb. 2010.

YIN KUANG received the bachelor's degree in electronic science and technology and the master's degree in communication and information engineering from Harbin Engineering University, Harbin, China, in 2007 and 2010, respectively.

He is currently a Senior Engineer with Xi'an Branch of China Academy of Space Technology, Xi'an, China. His research interests include radar and communication signal processing and satellite communication.

SHUXIAO LI is currently pursuing the B.E. degree with Southwest University of Science and Technology, Mianyang, China, in 2022. Her research interests include machine learning, communication signal processing, and wireless communication.

XUN HAN received the B.E. degree in electronic and information engineering and the Ph.D. degree in signal and information processing from Xidian University, Xi'an, China, in 2010 and 2015, respectively.

He is currently a Senior Engineer with Xi'an Branch of China Academy of Space Technology, Xi'an. His research interests include radar and communication signal processing, spectrum sensing, and covert communication.

WEI WEN received the B.E. degree in control technology and instrumentation and the Ph.D. degree in signal and information processing from Xidian University, Xi'an, China, in 2010 and 2016, respectively.

He is currently a Senior Engineer with Xi'an Branch of China Academy of Space Technology, Xi'an. His research interests include radar and communication signal processing, spectrum sensing, and laser communication.

YU WANG received the B.E. degree communication engineering and the master's degree in optical communication engineering from Xidian University, Xi'an, China, in 2011 and 2014, respectively.

He is currently an Intermediate Engineer with Xi'an Branch of China Academy of Space Technology, Xi'an. His research interests include signal transmission and communication signal processing.

MINGYU LI (Member, IEEE) received the Ph.D. degree in electronic engineering from the University of Electronic Science and Technology of China (UESTC), Chengdu, China, in 2009.

From 2012 to 2013, he was a Research Fellow with The University of Kitakyushu, Kitakyushu, Japan. He is currently a Full Professor with the School of Microelectronics and Communication Engineering, Chongqing University, Chongqing, China. His current research interests include RF/microwave circuits and systems designs, power management integrated circuits, satellite communication and systems, and behavioral modeling and linearization for RF power amplifiers.